HIGH RESOLUTION KRYLOV SPACE 3-D WAVENUMBER-FREQUENCY ANALYSIS *

Hongya Ge[1] *and Ivars P. Kirsteins*[2]

[1] Dept. of ECE, New Jersey Institute of Technology, Newark, NJ 07102, USA.
[2] Naval Undersea Warfare Center, Newport, RI 02841, USA.

ABSTRACT

Driven by the need for identifying the presence of flow noise components in a towed volumetric acoustic array, methodologies are developed for high resolution 3-dimensional (3-D) wavenumber-frequency (*k-f*) analysis based on Krylov space techniques. These methods are applied to actual noise data from a sea trial. The experimental results indicate that the Krylov-based method outperforms conventional approaches and provides efficient and effective solutions to *k-f* analysis.

Index Terms— Sonar Signal Processing, Array Signal Processing, Sonar Imaging, Krylov Space.

1. INTRODUCTION AND BACKGROUND

In order to reduce the interfering effects of noise radiated by the platform ship, passive and active sonar systems generally utilize arrays of hydrophones mounted on a cable that are towed behind the ship as their receivers. Besides waterborne acoustic noise (e.g. ambient noise, tow ship, shipping, biologics etc.), another important source of noise or interference present in towed arrays is flow noise. Flow noise is non-acoustic in nature and is caused by boundary layer turbulence exciting the array structure (including excitation of flexural-like waves in the array hose wall) and inducing pressure fluctuations on the surface of the hydrophones [1, 2]. Flow noise can significantly degrade sonar performance, e.g. probability of target signal detection, especially at high tow speeds. Therefore its presence and properties are of much interest to sonar system designers.

This work is motivated by the problem of identifying the presence of flow noise in a small sparsely-sampled volumetric array. Much insight into the types of noise present in an acoustic array can be obtained by performing a wavenumber-frequency (*k-f*) analysis of the space-time noise field measured by the array as it is towed through the water. A volumetric array requires 3-D wavenumber analysis as a function of frequency because of the 3-D arrangement of hydrophones. Hence we begin by reviewing 3-D *k-f* analysis.

Let $P(\mathbf{p}_m, t)$ denote the signal (acoustic and flow noise) time series measured at time t by the m-th hydrophone located at position $\mathbf{p}_m$. Then the wavenumber-frequency power spectrum is defined as the expected value

$$P(\mathbf{k}, f) = E\left\{ \left| \sum_m \int P(\mathbf{p}_m, t) e^{-j2\pi(\mathbf{k}^T \mathbf{p}_m - ft)} dt \right|^2 \right\}. \quad (1)$$

Or equivalently,

$$P(\mathbf{k}, f) = \mathbf{e}^H(\mathbf{k})\, \mathbf{R}[f]\, \mathbf{e}(\mathbf{k}), \quad (2)$$

where $\mathbf{e}^H(\mathbf{k}) = [\, e^{j2\pi\mathbf{k}^T\mathbf{p}_1}\ e^{j2\pi\mathbf{k}^T\mathbf{p}_2}\ \cdots e^{j2\pi\mathbf{k}^T\mathbf{p}_M}\,]$ is a 3-D wavenumber steering vector; vector $\mathbf{p}_m$ contains 3-D position coordinates of the m-th array element, and $\mathbf{R}[\mathbf{f}]$ is the nominal spatial covariance matrix of the noise field measured by the array at frequency f. In the above equations, the 3-D wavenumber vector $\mathbf{k} = [k_x\ k_y\ k_z]^T$ is defined in a Cartesian coordinate system. In this paper, k_x is always measured down the array axis. From formula (2) we see that the wavenumber-frequency spectrum is nothing more than a three-dimensional spatial Fourier analysis of the measured hydrophone signatures as a function of temporal frequency.

The structure of the wavenumber-frequency power spectrum is highly revealing about the types of noise sources present. This is best illustrated using a equi-spaced line array example which needs only a 1-D *k-f* analysis, that is, as a function of k_x and f. When the array elements are separated in distance by d, all plane wave acoustic signals must all lie in the *k-f* cone depicted in fig. 1. The region within the cone is known

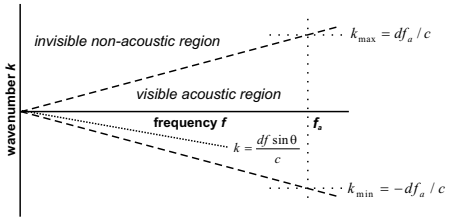

Fig. 1. Idealized $k-f$ spectrum: acoustic and non-acoustic regions.

as the visible acoustic region. For example, an acoustic plane wave signal impinging upon the array from direction θ will manifest itself as a ridge-like structure that lies within the acoustic cone as shown in fig. 1. Far field acoustic noise also lies within the acoustic cone or visible region. However, non-acoustic noise components such as flow noise will be present outside the acoustic cone and often has a ridge-like structure. Hence the presence of non-acoustic noise in an array can often

*THIS WORK HAS BEEN SUPPORTED IN PART BY THE ONR AND THE NSF (CCF-0515061).

Report Documentation Page

Form Approved
OMB No. 0704-0188

1. REPORT DATE	2. REPORT TYPE	3. DATES COVERED
2007		**00-00-2007 to 00-00-2007**

4. TITLE AND SUBTITLE	5a. CONTRACT NUMBER
High Resolution KRYLOV Space 3-D Wavenumber-Frequency Analysis	5b. GRANT NUMBER
	5c. PROGRAM ELEMENT NUMBER
6. AUTHOR(S)	5d. PROJECT NUMBER
	5e. TASK NUMBER
	5f. WORK UNIT NUMBER
7. PERFORMING ORGANIZATION NAME(S) AND ADDRESS(ES)	8. PERFORMING ORGANIZATION REPORT NUMBER
Dept. of ECE,New Jersey Institute of Technology,Newark,NJ,07102	
9. SPONSORING/MONITORING AGENCY NAME(S) AND ADDRESS(ES)	10. SPONSOR/MONITOR'S ACRONYM(S)
	11. SPONSOR/MONITOR'S REPORT NUMBER(S)

12. DISTRIBUTION/AVAILABILITY STATEMENT

Approved for public release; distribution unlimited

13. SUPPLEMENTARY NOTES

See also ADM002013. Proceedings of the 2007 IEEE International Conference on Acoustics, Speech, and Signal Processing (ICASSP), Held in Honolulu, Hawaii on April 15-20, 2007. Government or Federal Rights

14. ABSTRACT

15. SUBJECT TERMS

16. SECURITY CLASSIFICATION OF:			17. LIMITATION OF ABSTRACT	18. NUMBER OF PAGES	19a. NAME OF RESPONSIBLE PERSON
a. REPORT	b. ABSTRACT	c. THIS PAGE			
unclassified	**unclassified**	**unclassified**	**Same as Report (SAR)**	**4**	

be quickly determined by performing a simple wavenumber-frequency analysis. Similar results apply to a volumetric array except that the visible acoustic region now forms a 4-D hypercone in the space defined by the coordinates k_x, k_y, k_z, and f.

Estimating the *k-f* spectrum from real at-sea data is hard. Real acoustic data is often contaminated by acoustic interference such as that arising from the tow ship (as a result, sidelobe leakage from interferers can obscure weaker *k-f* features) and can be non-stationary because of array motion. In the case of a volumetric array, an especially challenging problem is visualization of the 4-D *k-f* volume on a 2-D display.

In the remainder of the paper, we develop a Krylov space-based high resolution *k-f* spectrum estimator and apply it to actual at-sea data collected from a volumetric array to identify the presence of flow noise. The Krylov-based high resolution estimator is compared against the periodogram and Capon's method [4] and is shown to work well. We also discuss and demonstrate methods for visualizing the 4-D *k-f* volume using slices of the spectrum taken in a spherical coordinate system.

2. PROPOSED SOLUTIONS AND RESULTS

The array of interest is comprised of triplet sets of hydrophones that are arranged and mounted in a triangular-like pattern (see fig. 2) on semi-rigid supports that are embedded in a hose-like structure. Unlike a conventional line array, the volumetric arrangement of hydrophones permits unambiguous left-right identification of acoustic sources.

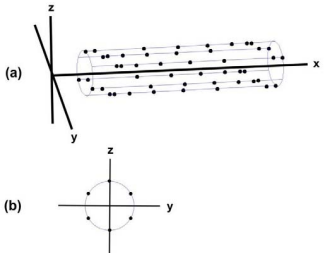

Fig. 2. Schematic diagram of the volumetric array; (a) Full view. (b) View down the array axis.

The conventional periodogram-based method generates a 4-D (3-D in space or wavenumber and 1-D in temporal frequency) volume revealing the wavenumber-frequency distribution of signal modes. That is,

$$P_{PER}(\mathbf{k}, f, t) = \mathbf{e}^H(\mathbf{k})\, \hat{\mathbf{R}}[f, t]\, \mathbf{e}(\mathbf{k}). \qquad (3)$$

Different from eq.(2), here $\hat{\mathbf{R}}[f, t]$ is a time-varying sample spatial covariance (the corss-spectral density matrix CSDM) obtained from *a finite number* of array noise measurements. It will be helpful for the purposes of visualizing the 4-D *k-f* volume to represent the wavenumber vector defined in eq. (1) using spherical coordinates as $\mathbf{k} = k\, \mathbf{u}(\phi, \theta)$ where $\mathbf{u}(\phi, \theta) = [\sin\theta\cos\phi \quad \sin\theta\sin\phi \quad \cos\theta]^T$ is the directional cosine vector as a function of the angles θ and ϕ. When the physical wavenumber $\|\mathbf{k}\|_F = k$ lies within the visible acoustic region at a given frequency, the angles ϕ and θ correspond to the actual azimuthal and elevation angles respectively of an acoustic signal impinging upon the array.

High levels of side-lobe leakage and limited resolution power associated with periodogram approach affects the performance of wavenumber-frequency analysis in revealing useful spatial modes and flow noise, especially when strong tow-ship interference is present in the estimated CSDM $\hat{\mathbf{R}}[f, t]$. Fig. 3(a) shows a 2-D slice cut out of the 4-D *k-f* volume in (3) obtained by setting $(\theta, \phi) = (90^o, 0^o)$ and plotting wavenumber k versus frequency f in the spherical coordinate system (this is equivalent to scanning k_x versus frequency while setting $k_y = k_z = 0$). The strong ridge-like feature present in the *k-f* spectrum that roughly follows the lower dashed line is radiated noise from the tow ship. The weaker ridges in the same orientation in the acoustic and non-acoustic regions are a result of sidelobes. This clearly illustrates the deleterious effects of side-lobe leakage of periodogram-like approaches.

Greatly improved performance in terms of sidelobe leakage and resolution can be obtained by using a high resolution spectral estimation method such as Capon's method [4]. Capon's method can be directly applied to estimate the 4-D wavenumber-frequency volume,

$$P_{CAPON}(\mathbf{k}, f, t) = \frac{1}{\mathbf{e}^H(\mathbf{k})\, \hat{\mathbf{R}}^{-1}[f, t]\, \mathbf{e}(\mathbf{k})}. \qquad (4)$$

However, inverting the $\hat{\mathbf{R}}[f, t]$ with a large eigen-spread will result in mode smearing and focusing problems. Shown in Fig. 3(b) is a 2-D slice of k-f spectrum from the 4-D k-f analysis results ($(\theta, \phi) = (90^o, 0^o)$) using Capon's method in eq. (4). Although greatly improved sidelobe leakage over the periodogram, we will show in the next section that even better performance can be attained using vector conjugate gradient (V-CG) rank-reduction approaches.

2.1. Improving performance using V-CG rank-reduction

In [8], motivated by the problem of adaptively detecting a signal using an array with a large number of sensors, we advocated using a Krylov subspace-based adaptive dimensionality reduction technique to improve detection performance and reduce sensitivity to model order uncertainty. In this application we are using the array manifold vector to scan the 3-D wavenumber space to reveal interesting activities. Roughly, only those noise and interference spatial modes (both acoustic and non-acoustic) that are not orthogonal to the steering replica or array manifold are relevant to estimating the spectrum at that direction. Such observation motivates us to propose and study an effective procedure that directly formulates a subspace for capturing only the spatial modes relevant to a given steering vector pointing to a direction of interest, i.e., rank reduction. Therefore, to alleviate resolution problems caused by inverting a high-dimensional CSDM $\hat{\mathbf{R}}[f, t]$ with a large eigen-spread, we propose using rank reduction based on the V-CG method. One then projects the estimated CSDM $\hat{\mathbf{R}}[f, t]$ onto the V-CG estimated subspace to yield an improved structural estimate of the CSDM for wavenumber-frequency analy-

sis. Therefore, we can directly use the V-CG method in formulating the projected structural estimate of CSDM, yet at the same time to control the rank of the space-time V-CG filter to avoid troubles caused by the large eigen-spreads of the sample estimate $\hat{\mathbf{R}}[f,t]$. Hence, a sequence of 4-D rank-r wavenumber-frequency spectra can be obtained using a rank-r V-CG method,

$$P_{VCG}^{(rank-r)}(\mathbf{k},f,t) = \frac{1}{\mathbf{e}^H(\mathbf{k})\,\mathbf{w}_r(\mathbf{k},f,t)}, \qquad (5)$$

where the rank-r V-CG space-time filter vector $\mathbf{w}_r(\mathbf{k},f,t)$ is constructed out of the Krylov space according to

$$\mathbf{w}_r(\mathbf{k},f,t) = \sum_{i=1}^{r} \alpha_i\,\mathbf{d}_i \in \mathcal{K}_r\{\hat{\mathbf{R}}[f,t],\mathbf{e}(\mathbf{k})\}, \qquad (6)$$

with Krylov space $\mathcal{K}_r\{\hat{\mathbf{R}},\mathbf{e}\} =< \mathbf{e},\hat{\mathbf{R}}\,\mathbf{e},\cdots,\hat{\mathbf{R}}^{r-1}\,\mathbf{e} >$. In the above V-CG space-time filter formulation, the conjugate direction vectors $\mathbf{d}_i$ and combination coefficients α_i are adaptively calculated from the estimated CSDM and the array manifold specified steering vector, without matrix inversion, using an iterative procedure [7]:

- initialization:

$$\mathbf{d}_1 = \mathbf{g}_1 = \mathbf{e}(\mathbf{k})$$

$$\mathbf{w}_1(\mathbf{k},f,t) = \alpha_1\,\mathbf{d}_1,\ \text{with}\ \alpha_1 = \frac{\mathbf{d}_1^H\mathbf{e}(\mathbf{k})}{\mathbf{d}_1^H\,\hat{\mathbf{R}}[f,t]\,\mathbf{d}_1}.$$

- refinement iterations $(i = 2,3,\ldots,r)$:

$$\mathbf{g}_i = \mathbf{g}_{i-1} + \hat{\mathbf{R}}[f,t]\,\mathbf{d}_{i-1}\,\alpha_{i-1},\ \text{gradient vectors}$$

$$\mathbf{d}_i = \mathbf{g}_i + \mathbf{d}_{i-1}\,\|\mathbf{g}_i\|^2/\|\mathbf{g}_{i-1}\|^2,\ \text{conjugate directions}$$

$$\alpha_i = \mathbf{d}_i^H\,\mathbf{e}(\mathbf{k})/(\mathbf{d}_i^H\,\hat{\mathbf{R}}[f,t]\,\mathbf{d}_i),\ \text{step-size.}$$

We further point out that the rank-r V-CG *k-f* spectrum in (5) can be interpreted as a Capon's k-f spectrum (without matrix inversion) in a reduced r-dimensional Krylov space. That is,

$$P_{VCG}^{(rank-r)} = \frac{1}{\mathbf{e}^H(\mathbf{k})\,\mathbf{D}_r\,(\mathbf{D}_r^H\hat{\mathbf{R}}[f,t]\mathbf{D}_r)^{-1}\,\mathbf{D}_r^H\,\mathbf{e}_(\mathbf{k})} \qquad (7)$$

$$= \frac{1}{\sum_{i=1}^{r}|\mathbf{d}_i^H\mathbf{e}(\mathbf{k})|^2/(\mathbf{d}_i^H\hat{\mathbf{R}}[f,t]\mathbf{d}_i)} \qquad (8)$$

with $\mathbf{D}_r = [\mathbf{d}_1,\mathbf{d}_2,\cdots,\mathbf{d}_r]$. Hence the reduced-dimension CSDM becomes $\hat{\mathbf{R}}_{\mathbf{D}}[f,t] = \mathbf{D}_r^H\,\hat{\mathbf{R}}[f,t]\,\mathbf{D}_r$. Here the dimensionality reduction matrix helps to alleviate the large eigen-spreads in the original full dimensional CSDM by re-shaping and subsequently truncating the eigen-values of the original CSDM $\hat{\mathbf{R}}[f,t]$, without incurring any loss in signal detection performance as long as $< \mathbf{D}_r >$ captures the spatial modes relevant to the steering vector $\mathbf{e}(\mathbf{k})$. In many applications, the dimensionality of subspace $< \mathbf{D}_r >$ can be much less than the array dimensionality N, and as a result, adaptive *k-f* analysis and adaptive beamformers may have greatly improved resolution performance due to the re-shaping and truncation on the widely spread eigen-values of the estimated CSDM $\hat{\mathbf{R}}[f,t]$. Formula (8) also reveals an interesting fact that the rank-*r* V-CG *k-f* spectrum can be viewed as a weighted harmonic average of *r* periodogram *k-f* spectra, each obtained by a "steering vector" defined by a conjugate direction vector.

2.2. Data results

In fig. 3(c) and fig.4(a), we demonstrate the high resolution results from our wavenumber-frequency analysis using the V-CG method($(\theta,\phi) = (90^o, 0^o)$) with rank 4 and 5. Fig. 4(b-c) show the *k-f* spectrum plotted for $(\theta,\phi) = (90^o, 90^o)$ and $(\theta,\phi) = (0^o, 90^o)$. As expected, the wavenumber resolution is much poorer now since we are scanning along the cross section dimensions of the array which are small relative to the signal wavelength. Results in figs. 3 and 4 demonstrate that the conventional method suffers severe side-lobe leakage from the tow-ship interference (parallel modes in k-f slice), while the Capon's method experiences mode smearing effect at low frequency region and loss of focus on spatial modes at high frequency region. Focused spatial modes can be seen across the frequency band of interest in the proposed V-CG method. It appears that most of the noise power is primarily concentrated in the acoustic region (marked by the white dashed lines) with little noise present in the non-acoustic region. This suggests that little flow noise is present in the array.

We also notice that the slowness spectrum provides a simple way of coherently consolidating the power distribution at different frequencies from the k-f spectrum. For a give 4D wavenumber-frequency function $P(\mathbf{k},f,t)$, the slowness spectrum can be extracted as,

$$P(\boldsymbol{\eta};f,t) = P(\mathbf{k},f,t,\text{such that}\ \boldsymbol{\eta} = \mathbf{k}/f). \qquad (9)$$

Fig. 5 shows the slowness spectra of a rank-5 V-CG method. Consistent peak locations in the slowness spectra acoustic region indicate that all acoustic modes are non-dispersive as expected.

3. DISCUSSION AND CONCLUSION

Further work is needed in effectively visualizing the 4-D *k-f* volume. Although "slicing" the spectrum along each of the x, y, and z wavenumber axis is highly revealing, it is plausible that some flow noise effects may have been missed as a result of this scanning scheme. Another approach is based on the observation that because of the cylindrical symmetry of the array (see fig. 2), there should be no "preferred" orientation of the wavenumber spectrum in the $y-z$ plane. Hence one could average out k_y and k_z by integrating around a circle of some fixed radius in the $y-z$ plane.

Finally, Krylov-based rank reduction V-CG methods provide significant improvements in performance over periodogram and Capon's methods when applied to real volumetric data.

4. REFERENCES

[1] D. Ross, "Mechanics of Underwater Noise," *Pergamon Press*, 1992.

[2] A. J. Shashaty, "The Effective Lengths for Flow Noise of Hydrophonesin a Ship-Towed Linear Array," *J. of Acoustic Soc. Am.*, 71(4), pp. 886–890, 1982.

[3] R. E. Zarnich, "A Fresh Look at 'Broadband' Passive Sonar Processing," *Proc. of the ASAP Workshop*, Lexington, MA, Mar. 1999.

[4] J. Capon, "High-Resolution Frequency-Wavenumber Spectrum Analysis," *Proc. IEEE,* vol. 57, Aug. 1969.
[5] M. E. Weippert, J. D. Hiemstra, J. S. Goldstein, and M. D. Zoltowski, "Insights from the Relationship between the Multistage Wiener Filter and the Method of Conjugate Gradients," *Proc. of IEEE SAM Workshop*, Washington, DC, Aug. 2002.
[6] L. L. Scharf, L. T. McWhorter, E. K. P. Chong, J. S. Goldstein, and M. D. Zoltowski, "Algebraic Equivalence of Conjugate Direction and Multistage Wiener Filters," *Proc. of the 11th Annual ASAP Workshop*, Lexington, MA, Mar. 2003.
[7] H. Ge, M. Lundberg, and L. L. Scharf, "Warp Convergence in Conjugate Gradient Wiener Filters," *Proc. of the 3rd IEEE SAM Workshop,* Barcelona, Spain, Jul. 2004.
[8] H. Ge, I. P. Kirsteins, and L. L. Scharf, "Data Dimension Reduction using Krylov Subspaces: Making Adaptive Beamformers Robust to Model Order-Determination," *Proc. of the IEEE ICASSP,* Toulouse, France, May 2006.

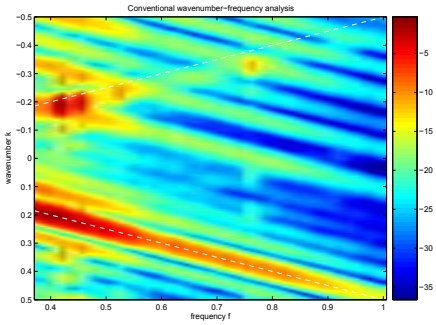

(a) Conventional method $P_{PER}(\mathbf{k}, f, t)$

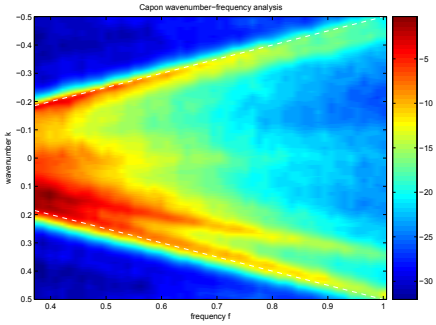

(b) Capon's method $P_{CAPON}(\mathbf{k}, f, t)$

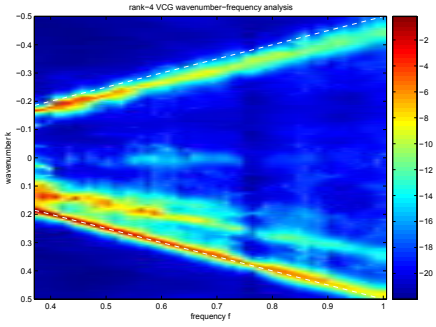

(c) Rank-4 VCG method $P_{VCG}^{(rank-4)}(\mathbf{k}, f, t)$

Fig. 3. 2D k-f slices out of 4D wavenumber-frequency spectrum estimates from different methods, at a fixed time slot and a fixed spatial direction $(\theta, \phi) = (90^o, 0^o)$.

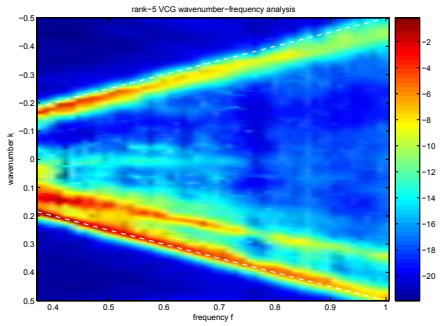

(a) $P_{VCG}^{(rank-5)}(\mathbf{k}, f, t)$, viewing in k_x direction.

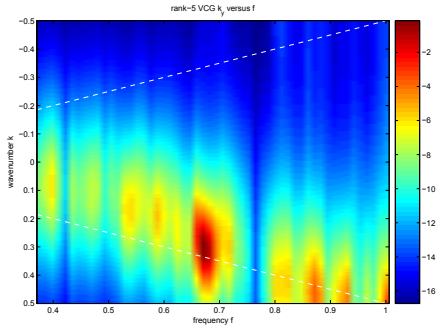

(b) $P_{VCG}^{(rank-5)}(\mathbf{k}, f, t)$, viewing in k_y direction.

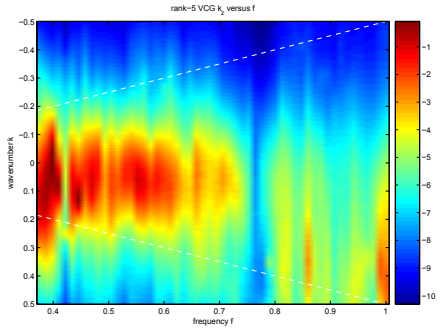

(c) VCG $P_{VCG}^{(rank-5)}(\mathbf{k}, f, t)$, viewing in k_z direction.

Fig. 4. 2D k-f slices out of 4D wavenumber-frequency spectrum estimate from a rank-5 V-CG method, at fixed spatial directions. (a) k_x direction $(\theta, \phi) = (90^o, 0^o)$; (b) k_y direction $(\theta, \phi) = (90^o, 90^o)$; (c) k_z direction $(\theta, \phi) = (0^o, 90^o)$.

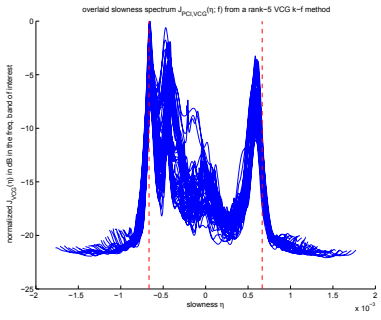

Fig. 5. Overlaid slowness spectra extracted from a rank-5 VCG 4D k-f spectrum on the 3D volumetric data, over the frequency band of interest. Acoustic region is marked by red dashed lines.